Comprehensive Extrinsic Calibration of a Camera and a 2D Laser Scanner for a Ground Vehicle

Hao LI, Fawzi NASHASHIBI

TECHNICAL REPORT

N° 438

July 2013

Project-Team IMARA

ISSN 0249-6399 ISRN INRIA/RT--438--FR+ENG

Comprehensive Extrinsic Calibration of a Camera and a 2D Laser Scanner for a Ground Vehicle

Hao LI*, Fawzi NASHASHIBI†

Project-Team IMARA

Technical Report N° 438 — July 2013 — 24 pages

Abstract: Cameras and laser scanners are two important kinds of perceptive sensors and both become more and more commonly used for intelligent ground vehicles; the calibration of these sensors is a fundamental task. A new method is proposed to perform COMPREHENSIVE extrinsic calibration of a SINGLE camera-2D laser scanner pair, i.e. the process of revealing ALL the spatial relationships among the camera coordinates system, the laser scanner coordinates system, the ground coordinates system, and the vehicle coordinates system. The proposed method is mainly based on the convenient and widely used chessboard calibration practice and can be conveniently implemented. The proposed method has been tested on both synthetic data and real data based experiments, which validate the effectiveness of the proposed method.

Key-Words: Calibration, camera, 2D laser scanner, vehicle, mobile robot

* Hao LI: Imara, INRIA Paris-Rocquencourt, hao.li@inria.fr
†

RESEARCH CENTRE
ROCQUENCOURT

Domaine de Voluceau
Rocquencourt BP 105
78153 Le Chesnay Cedex France

Calibration Extrinsèque Compréhensive d'une Caméra et un Scanner Laser 2D pour un Véhicule Terrestre

Résumé : La caméra et le scanner laser sont deux types importants de capteurs perceptifs et tous les deux deviennent de plus en plus communs pour de nombreuses applications des véhicules intelligents. La calibration de ces capteurs est une tâche fondamentale. Dans ce rapport, on a propose une nouvelle méthode pour réaliser la calibration extrinsèque *compréhensive* d'une seule paire caméra-scanner laser 2D, à savoir le procédé de révéler tous les relations spatiales parmi un système de coordonnées caméra, un système de coordonnées scanner laser, un système de coordonnées terrestre, et un système de coordonnées véhicule. La méthode proposée se fonde principalement sur la practique de cabliration au damier et est facile à mettre en œuvre. Des tests des données réelles et des données synthétiques ont validé la performance de la méthode proposée.

Mots-Clés : Calibration, caméra, scanner laser 2D, véhicule, robot mobile

1 Introduction

Cameras and laser scanners are two important kinds of perceptive sensors and both become more and more commonly used for ground intelligent vehicle applications (or ground mobile robot applications). Given a vehicle equipped with a camera and a 2D laser scanner, it is sometimes needed to relate the data of one sensor to those of the other [1] [2] [3], to relate the sensor data to the ground plane [4], and to relate the sensor data to the vehicle [5] [6]. All these requirements concern a fundamental task of COMPREHENSIVE extrinsic calibration of a camera and a 2D laser scanner, i.e. the process of revealing ALL the spatial relationships among the camera coordinates system, the laser scanner coordinates system, the ground coordinates system, and the vehicle coordinates system.

There are two kinds of needs for the calibration of these sensors: one kind is from manufacturers who fabricate the vehicle platforms; the other kind is from researchers who use the vehicle platforms in *ad hoc* ways. The manufacturers normally possess special advanced equipments which can calibrate the installed sensors according to strict manufacturing standards; the installation of the sensors calibrated in this way is not intended to be changed after the calibration. On the other hand, the researchers might occasionally adjust the sensor installation for certain *ad hoc* tasks and thus need to re-calibrate the extrinsic parameters of the sensors. However, the researchers usually do not have the special calibration equipments as the manufacturers do. Therefore in this report, we only address calibration methods that are intended to satisfy the needs of the researchers.

Comparatively more published works deal with the extrinsic calibration of MULTIPLE camera-2D laser scanner pairs [7] [8] [9] [10] [11], i.e. the calibration concerning multiple cameras (including stereo-camera), or multiple 2D laser scanners (including 3D laser scanner), or concerning both. In contrast, the extrinsic calibration of SINGLE camera-2D laser scanner pair only concerns one camera and one 2D laser scanner. Compared with the calibration of multiple camera-2D laser scanner pairs, the calibration of single camera-2D laser scanner pair is more difficult, because less geometric constraints can be exploited to recover the extrinsic parameters. Besides, the calibration of single camera-2D laser scanner pair is more general and basic: it can be directly adapted for the calibration of multiple camera-2D laser scanner pairs, whereas the converse can not hold.

Concerning the extrinsic calibration of single camera-2D laser scanner pair, the number of published works is small; Zhang & Pless method [12] is the most widely used method, thanks to its convenience and its generality: this method is based on the

convenient chessboard calibration practice that has almost become a standard routine for camera intrinsic calibration since the introduction of this practice by Zhang Z. [13]; it does not require complex calibration conditions, such as IMU devices [7] or complicated calibration boards [14]. Zhang & Pless method can be applied to the calibration of any general camera-2D laser scanner pair, unlike some methods that work only for certain special kind of laser scanners (such as visible laser scanner [19]). Since this report also handles the extrinsic calibration of single camera-2D laser scanner pair and intends providing a convenient and general solution, Zhang & Pless method [12] serves as a proper reference method for our presented works.

A new calibration method which aims at performing comprehensive extrinsic calibration of a camera and a 2D laser scanner is proposed. The contribution of the proposed method mainly lies in the following aspects:

1) The proposed method can reveal ALL the spatial relationships among the camera coordinates system, the laser scanner coordinates system, the ground coordinates system, and the vehicle coordinates system, based on the chessboard calibration practice with few extra measurements.

2) The proposed method yields two improvements over the reference method in [12], even based exactly on the same chessboard calibration practice. First, the proposed method can reveal more spatial relationships than the method in [12] does. More specifically, the method in [12] only reveals the spatial relationship between a camera and a 2D laser scanner, whereas the proposed method can not only reveal this spatial relationship but also that between the two sensors and the ground plane. Second, the proposed method outperforms the method in [12] in terms of calibration accuracy, even only concerning the extrinsic calibration between the camera and the 2D laser scanner.

2 Mathematical Fundaments and Denotations

Several coordinates systems are relevant in the presentation of the proposed method: the camera coordinates system (CCS), the laser scanner coordinates system (SCS), the ground coordinates system (GCS), the vehicle coordinates system (VCS), and the chessboard plane coordinates system (PCS).

The origin and the coordinate axes of the CCS are denoted by $\{\mathbf{O_c},\mathbf{X_c},\mathbf{Y_c},\mathbf{Z_c}\}$, where the $\mathbf{O_c}$-$\mathbf{X_c}$-$\mathbf{Y_c}$ plane is parallel to the image plane. The origin and the coordinate axes of the SCS are denoted by $\{\mathbf{O_s},\mathbf{X_s},\mathbf{Y_s},\mathbf{Z_s}\}$, where the plane $\mathbf{Z_s}$=0 is the scanning plane of the 2D laser scanner.

Let the vehicle be stationary on the ground plane, the GCS and VCS are established as follows: the origin and the coordinate axes of the VCS are denoted by $\{\mathbf{O_v},\mathbf{X_v},\mathbf{Y_v},\mathbf{Z_v}\}$, where the $\{\mathbf{X_v},\mathbf{Y_v},\mathbf{Z_v}\}$ are respectively along the longitudinal direction, the lateral

direction, and the vertical direction of the vehicle; the $\mathbf{O_v}$ is at the ground projection of the rear wheel axle center. The origin and the coordinate axes of the GCS are denoted by $\{\mathbf{O_g},\mathbf{X_g},\mathbf{Y_g},\mathbf{Z_g}\}$, where the $\mathbf{O_g}$ is at the ground projection of the $\mathbf{O_c}$, the $\mathbf{Z_g}$ points from the $\mathbf{O_g}$ to the $\mathbf{O_c}$; the $\mathbf{X_g}$ is along the ground projection of the $\mathbf{Z_c}$.

Given a pose of the chessboard plane, the origin and the coordinate axes of the PCS are denoted by $\{\mathbf{O_p},\mathbf{X_p},\mathbf{Y_p},\mathbf{Z_p}\}$, where the plane $\mathbf{Z_p}=0$ is situated on the chessboard plane, the $\mathbf{O_p}$ is at the chessboard left-bottom corner, the $\mathbf{X_p}$ is along the chessboard bottom edge, and the $\mathbf{Y_p}$ is along the chessboard left edge. The chessboard is placed with several different poses in the perception field of the camera and the 2D laser scanner; for each pose, a sub-script '$_{(i)}$' is used to distinguish the PCS. Thus the different chessboard poses that are used for calibration are denoted by a set of $PCS_{(i)}$, i.e. $PCS_{(1)}\{\mathbf{O_{p(1)}},\mathbf{X_{p(1)}},\mathbf{Y_{p(1)}},\mathbf{Z_{p(1)}}\}$, $PCS_{(2)}\{\mathbf{O_{p(2)}},\mathbf{X_{p(2)}},\mathbf{Y_{p(2)}},\mathbf{Z_{p(2)}}\}$, … An illustration of these coordinates systems is given in Fig.1.

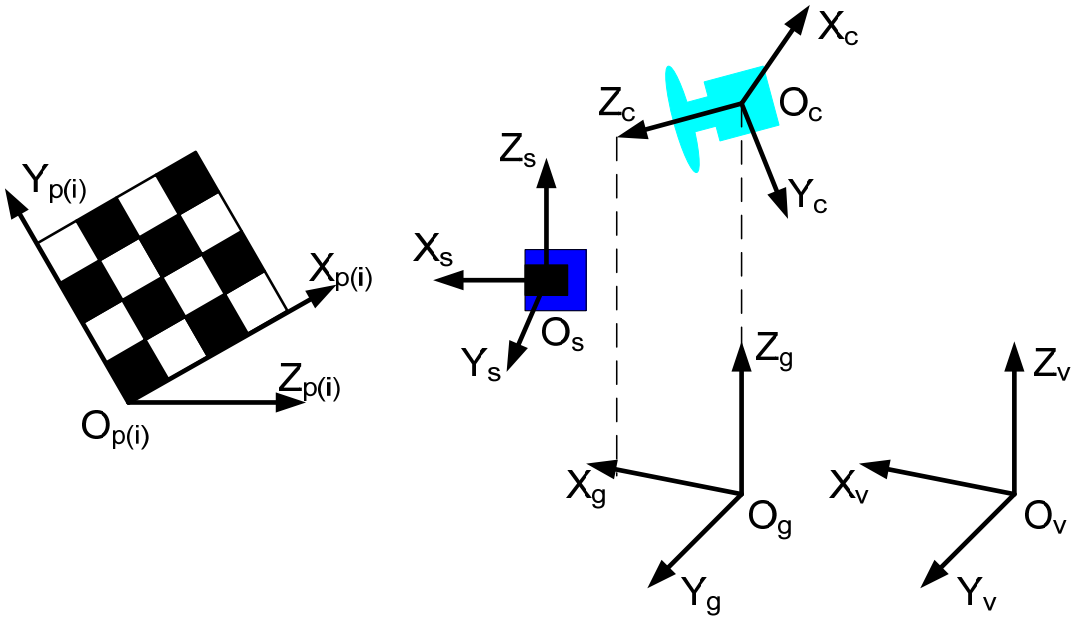

Fig.1. The coordinates systems: CCS, SCS, GCS, VCS, and $PCS_{(i)}$

It is worthy noting that these coordinates systems might be established differently; they are established in above way mainly for calibration convenience and possible applications associated with ground vehicles (or ground mobile robots).

In this report, the $\{\mathbf{X_a},\mathbf{Y_a},\mathbf{Z_a}\}$ also denote the unit vectors along corresponding coordinate axes. The '**R**' and '**T**' generally denote 3×3 rotation matrix and 3×1 translation vector respectively. The '$\mathbf{R_{ab}}$' and '$\mathbf{T_{ab}}$' denote the rotation and translation

from the coordinates system $\{\mathbf{O_a},\mathbf{X_a},\mathbf{Y_a},\mathbf{Z_a}\}$ to the coordinates system $\{\mathbf{O_b},\mathbf{X_b},\mathbf{Y_b},\mathbf{Z_b}\}$. For example, '$\mathbf{R_{cs}}$' and '$\mathbf{T_{cs}}$' denote the transformation from the CCS to the SCS. The '**M**' denotes a point and $\mathbf{M_a}=[x_a,y_a,z_a]^T$ denotes the coordinates of '**M**' in $\{\mathbf{O_a},\mathbf{X_a},\mathbf{Y_a},\mathbf{Z_a}\}$. The following relationships always hold (**a**,**b**,**f**={c, s, g, v, p(1), p(2), …}):

$$\mathbf{M_b} = \mathbf{R_{ab}}\mathbf{M_a} + \mathbf{T_{ab}}$$

Dual relationship: $\mathbf{R_{ba}} = \mathbf{R_{ab}}^{\mathbf{T}}; \mathbf{T_{ba}} = -\mathbf{R_{ab}}^{\mathbf{T}}\mathbf{T_{ab}}$ (1a)

Chain relationship: $\mathbf{R_{ab}} = \mathbf{R_{fb}}\mathbf{R_{af}}; \mathbf{T_{ab}} = \mathbf{R_{fb}}\mathbf{T_{af}} + \mathbf{T_{fb}}$ (1b)

In the CCS, the '$\mathbf{N_{p(i)c}}$' is used to denote the perpendicular vector from the $\mathbf{O_c}$ to the plane $PCS_{(i)}$. The '$\mathbf{N_{gc}}$' is used to denote the perpendicular vector from the $\mathbf{O_c}$ to the ground plane. Let $\mathbf{N_{Gc}}=[\mathbf{N_{gc}}^T,n_0]^T$ and let the ground plane be represented by equation $\mathbf{N_{Gc}}^T[\mathbf{M_c}^T,1]^T=0$.

A List of notations is summarized as follows:

$\{\mathbf{O_c},\mathbf{X_c},\mathbf{Y_c},\mathbf{Z_c}\}$	Camera Coordinates System (CCS)
$\{\mathbf{O_s},\mathbf{X_s},\mathbf{Y_s},\mathbf{Z_s}\}$	Laser Scanner Coordinates System (SCS)
$\{\mathbf{O_v},\mathbf{X_v},\mathbf{Y_v},\mathbf{Z_v}\}$	Vehicle Coordinates System (VCS)
$\{\mathbf{O_g},\mathbf{X_g},\mathbf{Y_g},\mathbf{Z_g}\}$	Ground Coordinates System (GCS)
R and **T**	Rotation and Translation (general)
$\mathbf{R_{ab}}$	**R** from $\{\mathbf{O_a},\mathbf{X_a},\mathbf{Y_a},\mathbf{Z_a}\}$ to $\{\mathbf{O_b},\mathbf{X_b},\mathbf{Y_b},\mathbf{Z_b}\}$
$\mathbf{T_{ab}}$	**T** from $\{\mathbf{O_a},\mathbf{X_a},\mathbf{Y_a},\mathbf{Z_a}\}$ to $\{\mathbf{O_b},\mathbf{X_b},\mathbf{Y_b},\mathbf{Z_b}\}$
M	A point (general)
$\mathbf{M_a}=[x_a,y_a,z_a]^T$	A point **M** in $\{\mathbf{O_a},\mathbf{X_a},\mathbf{Y_a},\mathbf{Z_a}\}$.
$\mathbf{N_{p(i)c}}$	(In CCS) the perpendicular vector from $\mathbf{O_c}$ to the plane $PCS_{(i)}$.
$\mathbf{N_{gc}}$	(In CCS) the perpendicular vector from $\mathbf{O_c}$ to the ground plane.
$\mathbf{N_{Gc}}=[\mathbf{N_{gc}}^T,n_0]^T$	Given a generic point $\mathbf{M_c}$ on the ground plane, then $\mathbf{N_{Gc}}^T[\mathbf{M_c}^T,1]^T=0$.
$\mathbf{e_1}$, $\mathbf{e_2}$, and $\mathbf{e_3}$	$[1,0,0]^T$, $[0,1,0]^T$, and $[0,0,1]^T$.
L2-norm ‖.‖	Given an arbitrary vector **V**, $\|\mathbf{V}\|^2=\mathbf{V^TV}$.

3 The Basic Version of the Comprehensive Extrinsic Calibration Method

The whole calibration method consists of three parts: 1) the method [12] to perform the calibration between the CCS and the SCS (briefly reviewed), based on the chessboard calibration practice; 2) a proposed method to perform the calibration between the CCS and the GCS, based on the same chessboard calibration practice; 3) a proposed method to perform the calibration between the GCS and the VCS, with the help of few extra measurements in addition to the chessboard calibration practice.

3.1 The Calibration Between the CCS and the SCS

The camera intrinsic parameters are calibrated using the method in [13]; given several chessboard poses for calibration: $PCS_{(1)}\{\mathbf{O}_{\mathbf{p}(1)},\mathbf{X}_{\mathbf{p}(1)}, \mathbf{Y}_{\mathbf{p}(1)}, \mathbf{Z}_{\mathbf{p}(1)}\}$, $PCS_{(2)}\{\mathbf{O}_{\mathbf{p}(2)},\mathbf{X}_{\mathbf{p}(2)}, \mathbf{Y}_{\mathbf{p}(2)}, \mathbf{Z}_{\mathbf{p}(2)}\}$, etc. For a pose $PCS_{(i)}$, the $\mathbf{N}_{\mathbf{p(i)c}}$ is computed as:

$$\mathbf{N}_{\mathbf{p(i)c}} = (\mathbf{e_3}^{\mathrm{T}}\mathbf{R}_{\mathbf{p(i)c}}{}^{\mathrm{T}}\mathbf{T}_{\mathbf{p(i)c}})\mathbf{R}_{\mathbf{p(i)c}}\mathbf{e_3}$$

$\mathbf{R}_{\mathbf{p(i)c}}$ and $\mathbf{T}_{\mathbf{p(i)c}}$ are computed via the homography between the plane $Z_{p(i)}=0$ and the image coordinates system [13].

According to the geometric constraint that laser points should be located on the chessboard plane, $\mathbf{R}_{\mathbf{cs}}$ and $\mathbf{T}_{\mathbf{cs}}$ are optimized by minimizing the summed square of distances of all the laser points to corresponding chessboard planes [12]:

$$\begin{aligned} &\{\mathbf{R}_{\mathbf{cs}}, \mathbf{T}_{\mathbf{cs}}\} = \arg\min_{\mathbf{R}_{\mathbf{cs}}, \mathbf{T}_{\mathbf{cs}}} F_1 \\ &F_1 = \sum_i \sum_j [\frac{\mathbf{N}_{\mathbf{p(i)c}}}{\| \mathbf{N}_{\mathbf{p(i)c}} \|} \cdot \mathbf{R}_{\mathbf{cs}}{}^{-1}(\mathbf{M}_{\mathbf{s(i,j)}} - \mathbf{T}_{\mathbf{cs}}) - \| \mathbf{N}_{\mathbf{p(i)c}} \|]^2 \end{aligned} \quad (2)$$

Where $\mathbf{R}_{\mathbf{cs}}$ is parameterized by a 3-vector using the Rodrigues formula [15]; $\mathbf{M}_{\mathbf{s(i,j)}}$ is the j-th laser point on the $PCS_{(i)}$. The initial values of $\mathbf{R}_{\mathbf{cs}}$ and $\mathbf{T}_{\mathbf{cs}}$ are estimated by solving a linear equation problem [12]. The $\mathbf{R}_{\mathbf{sc}}$ and $\mathbf{T}_{\mathbf{sc}}$ can be computed using the dual relationship (1a): $\mathbf{R}_{\mathbf{sc}}=\mathbf{R}_{\mathbf{cs}}{}^{\mathrm{T}}$; $\mathbf{T}_{\mathbf{sc}}=-\mathbf{R}_{\mathbf{cs}}{}^{\mathrm{T}}\mathbf{T}_{\mathbf{cs}}$.

3.2 The Calibration Between the CCS and the GCS

During the chessboard calibration practice, one can hold the chessboard either on the ground or in the air, only if the camera and the 2D laser scanner can both perceive the chessboard. In practice, it is more convenient and more stable to hold the chessboard on the ground than in the air, as the chessboard might be large and heavy.

Besides, posing the chessboard on the ground brings one more geometric constraint: *ground plane constraint*. It means that the chessboard bottom edge, i.e. the line $\mathbf{O}_{\mathbf{p}(i)}+\lambda\mathbf{X}_{\mathbf{p}(i)}$ (λ is a scalar), is situated on the ground plane. This constraint is reasonable, because a calibration field fairly flat could always be found; for example, on the floor in a garage room.

Let l be the length of the chessboard bottom edge; the corner points $\mathbf{O}_{\mathbf{p}(i)}$ and $\mathbf{O}_{\mathbf{p}(i)}+l\cdot\mathbf{X}_{\mathbf{p}(i)}$ are chosen as control points. The $\mathbf{R}_{\mathbf{p(i)c}}$ and $\mathbf{T}_{\mathbf{p(i)c}}$ are computed as mentioned in Section III.A. In the CCS, the coordinates of $\mathbf{O}_{\mathbf{p}(i)}$ and $\mathbf{X}_{\mathbf{p}(i)}$ are respectively $\mathbf{T}_{\mathbf{p(i)c}}$ and $\mathbf{R}_{\mathbf{p(i)c}}\mathbf{e_1}$. As the ground plane is denoted by $\mathbf{N}_{\mathbf{Gc}}{}^{\mathrm{T}}[\mathbf{M}_{\mathbf{c}}{}^{\mathrm{T}},1]^{\mathrm{T}}=0$, a linear equation can be established:

$$\mathbf{G}^{T}\mathbf{N}_{\mathbf{Gc}}=\mathbf{0} \tag{3}$$

$$\mathbf{G}=\begin{bmatrix}\cdots & \mathbf{T}_{\mathbf{p(i)c}} & \mathbf{T}_{\mathbf{p(i)c}}+l\cdot\mathbf{R}_{\mathbf{p(i)c}}\mathbf{e_1} & \cdots\\ \cdots & 1 & 1 & \cdots\end{bmatrix}$$

The $\mathbf{N}_{\mathbf{Gc}}$ is the eigenvector associated with the smallest eigenvalue of $\mathbf{GG}^{\mathbf{T}}$. Recall that $\mathbf{N}_{\mathbf{Gc}}=[\mathbf{N}_{\mathbf{gc}}{}^{\mathrm{T}},n_0]^{\mathrm{T}}$; the 3-vector $\mathbf{N}_{\mathbf{gc}}$ is perpendicular to the ground plane. The $\mathbf{R}_{\mathbf{gc}}$ and $\mathbf{T}_{\mathbf{gc}}$, are computed as follows:

$$\mathbf{T}_{\mathbf{gc}}=-\frac{n_0}{\|\mathbf{N}_{\mathbf{gc}}\|^2}\mathbf{N}_{\mathbf{gc}}$$

$$\mathbf{R}_{\mathbf{gc}}\mathbf{e_1}=\left(-\frac{\mathbf{N}_{\mathbf{gc}}{}^{\mathbf{T}}\mathbf{e_3}}{\|\mathbf{N}_{\mathbf{gc}}\|^2}\mathbf{N}_{\mathbf{gc}}+\mathbf{e_3}\right)/\left\|-\frac{\mathbf{N}_{\mathbf{gc}}{}^{\mathbf{T}}\mathbf{e_3}}{\|\mathbf{N}_{\mathbf{gc}}\|^2}\mathbf{N}_{\mathbf{gc}}+\mathbf{e_3}\right\|$$

$$\mathbf{R}_{\mathbf{gc}}\mathbf{e_3}=-\mathbf{T}_{\mathbf{gc}}/\|\mathbf{T}_{\mathbf{gc}}\|$$

$$\mathbf{R}_{\mathbf{gc}}\mathbf{e_2}=(\mathbf{R}_{\mathbf{gc}}\mathbf{e_3})\times(\mathbf{R}_{\mathbf{gc}}\mathbf{e_1})$$

$\mathbf{R}_{\mathbf{cg}}$ and $\mathbf{T}_{\mathbf{cg}}$ can be computed using the dual relationship (1a): $\mathbf{R}_{\mathbf{cg}}=\mathbf{R}_{\mathbf{gc}}{}^{\mathbf{T}}$; $\mathbf{T}_{\mathbf{cg}}=-\mathbf{R}_{\mathbf{gc}}{}^{\mathbf{T}}\mathbf{T}_{\mathbf{gc}}$. The spatial relationship between the SCS and the GCS can be computed using the chain relationship (1b): $\mathbf{R}_{\mathbf{sg}}=\mathbf{R}_{\mathbf{cg}}\mathbf{R}_{\mathbf{sc}}$; $\mathbf{T}_{\mathbf{sg}}=\mathbf{R}_{\mathbf{cg}}\mathbf{T}_{\mathbf{sc}}+\mathbf{T}_{\mathbf{cg}}$.

Proof:

Lemma: Given a plane denoted as $\mathbf{N}_{\mathbf{p}}{}^{\mathrm{T}}[\mathbf{M}^{\mathrm{T}},1]^{\mathrm{T}}=0$, where $\mathbf{N}_{\mathbf{p}}=[\mathbf{N}^{\mathrm{T}},n_0]^{\mathrm{T}}$ and $\mathbf{N}$ is a 3-vector; for an arbitrary point $\mathbf{M}_{\mathbf{a}}$, the projection of $\mathbf{M}_{\mathbf{a}}$ on this plane, denoted as $\mathbf{M}_{\mathbf{a(p)}}$, is computed as:

$$\mathbf{M}_{\mathbf{a(p)}}=-\frac{\mathbf{N}^{\mathbf{T}}\mathbf{M}_{\mathbf{a}}+n_0}{\|\mathbf{N}\|^2}\mathbf{N}+\mathbf{M}_{\mathbf{a}}$$

Lemma proof: As the 3-vector $\mathbf{N}$ is perpendicular to the plane, the projection $\mathbf{M}_{\mathbf{a(p)}}$ is in the form $\mathbf{M}_{\mathbf{a(p)}}=\mathbf{M}_{\mathbf{a}}+\lambda\mathbf{N}$ where λ is a scalar to-be-computed. Substitute $\mathbf{M}_{\mathbf{a(p)}}=\mathbf{M}_{\mathbf{a}}+\lambda\mathbf{N}$ for $\mathbf{M}$ in the equation $\mathbf{N}_{\mathbf{p}}{}^{\mathrm{T}}[\mathbf{M}^{\mathrm{T}},1]^{\mathrm{T}}=0$, i.e. $\mathbf{N}^{\mathrm{T}}(\mathbf{M}_{\mathbf{a}}+\lambda\mathbf{N})+n_0=0$, and compute the λ:

$$\lambda = -\frac{\mathbf{N}^{\mathbf{T}}\mathbf{M}_{\mathbf{a}} + n_0}{\mathbf{N}^{\mathbf{T}}\mathbf{N}} = -\frac{\mathbf{N}^{\mathbf{T}}\mathbf{M}_{\mathbf{a}} + n_0}{\| \mathbf{N} \|^2}$$

Substitute the λ into $\mathbf{M}_{\mathbf{a(p)}}=\mathbf{M}_{\mathbf{a}}+\lambda\mathbf{N}$ and the lemma is done. □

In the CCS, let the ground plane be denoted by equation $\mathbf{N}_{\mathbf{Gc}}{}^{\mathbf{T}}[\mathbf{M}_{\mathbf{c}}{}^{\mathrm{T}},1]^{\mathbf{T}}=0$ and the $\mathbf{N}_{\mathbf{Gc}}=[\mathbf{N}_{\mathbf{gc}}{}^{\mathrm{T}},n_0]^{\mathrm{T}}$. According to the establishment of the GCS as specified in section 2, the $\mathbf{O}_{\mathbf{g}}$ (i.e. $\mathbf{T}_{\mathbf{gc}}$ in the CCS) is the projection of the $\mathbf{O}_{\mathbf{c}}$ (i.e. $\mathbf{0}$ in the CCS) on the ground plane; then $\mathbf{T}_{\mathbf{gc}}$ can be computed via the lemma:

$$\mathbf{T}_{\mathbf{gc}} = -\frac{\mathbf{N}_{\mathbf{gc}}{}^{\mathbf{T}}\mathbf{0} + n_0}{\| \mathbf{N}_{\mathbf{gc}} \|^2}\mathbf{N}_{\mathbf{gc}} + \mathbf{0} = -\frac{n_0}{\| \mathbf{N}_{\mathbf{gc}} \|^2}\mathbf{N}_{\mathbf{gc}}$$

As the axis $\mathbf{Z}_{\mathbf{g}}$ points from $\mathbf{O}_{\mathbf{g}}$ to $\mathbf{O}_{\mathbf{c}}$, the unit vector $\mathbf{Z}_{\mathbf{g}}$ (i.e. $\mathbf{R}_{\mathbf{gc}}\mathbf{e}_{\mathbf{3}}$ in the CCS) is computed as:

$$\mathbf{R}_{\mathbf{gc}}\mathbf{e}_3 = -\mathbf{T}_{\mathbf{gc}} / \| \mathbf{T}_{\mathbf{gc}} \|$$

Select a point on the axis $\mathbf{Z}_{\mathbf{c}}$ (let it be $\mathbf{e}_{\mathbf{3}}$ in the CCS) and compute its projection on the ground plane:

$$\mathbf{P}_{\mathbf{z}} = -\frac{\mathbf{N}_{\mathbf{gc}}{}^{\mathbf{T}}\mathbf{e}_{\mathbf{3}} + n_0}{\| \mathbf{N}_{\mathbf{gc}} \|^2}\mathbf{N}_{\mathbf{gc}} + \mathbf{e}_{\mathbf{3}}$$

As the axis $\mathbf{X}_{\mathbf{g}}$ is along the projection of the axis $\mathbf{Z}_{\mathbf{c}}$ on the ground, the unit vector $\mathbf{X}_{\mathbf{g}}$ (i.e. $\mathbf{R}_{\mathbf{gc}}\mathbf{e}_{\mathbf{1}}$ in the CCS) is computed as:

$$\begin{aligned}\mathbf{R}_{\mathbf{gc}}\mathbf{e}_{\mathbf{1}} &= (\mathbf{P}_{\mathbf{z}} - \mathbf{T}_{\mathbf{gc}}) / \| \mathbf{P}_{\mathbf{z}} - \mathbf{T}_{\mathbf{gc}} \| \\ &= (-\frac{\mathbf{N}_{\mathbf{gc}}{}^{\mathbf{T}}\mathbf{e}_{\mathbf{3}}}{\| \mathbf{N}_{\mathbf{gc}} \|^2}\mathbf{N}_{\mathbf{gc}} + \mathbf{e}_{\mathbf{3}}) / \| -\frac{\mathbf{N}_{\mathbf{gc}}{}^{\mathbf{T}}\mathbf{e}_{\mathbf{3}}}{\| \mathbf{N}_{\mathbf{gc}} \|^2}\mathbf{N}_{\mathbf{gc}} + \mathbf{e}_{\mathbf{3}} \|\end{aligned}$$

According to the right-hand rule, the unit vector $\mathbf{Y_g}$ (i.e. $\mathbf{R_{gc}e_2}$ in the CCS) is computed as:

$$\mathbf{R_{gc}e_2} = (\mathbf{R_{gc}e_3}) \times (\mathbf{R_{gc}e_1})$$

□

3.3 The Calibration Between the GCS and the VCS

The transformation between the GCS and the VCS is given by a rotation around the axis $\mathbf{Z_g}$ and a translation along the ground plane, as follows:

$$\begin{bmatrix} x_v \\ y_v \\ z_v \end{bmatrix} = \begin{bmatrix} \cos\theta & -\sin\theta & 0 \\ \sin\theta & \cos\theta & 0 \\ 0 & 0 & 1 \end{bmatrix} \begin{bmatrix} x_g \\ y_g \\ z_g \end{bmatrix} + \begin{bmatrix} t_x \\ t_y \\ 0 \end{bmatrix} \quad (4)$$

Given a $PCS_{(i)}$, the $\mathbf{O_{p(i)}}$ is chosen as a *ground control point*. The coordinates of $\mathbf{O_{p(i)}}$ in the GCS is computed as: $\mathbf{O_{p(i)g}}=\mathbf{R_{cg}T_{p(i)c}}+\mathbf{T_{cg}}$. Choose some ground control points $\mathbf{O_{p(i)}}$, compute their coordinates $\mathbf{O_{p(i)g}}=[x_{og(i)},y_{og(i)}]^T$ in the GCS, and measure their coordinates $\mathbf{O_{p(i)v}}=[x_{ov(i)},y_{ov(i)}]^T$ in the VCS. Since $z_v=z_g$ always holds here, the third coordinate is omitted.

With all the pairs of control points, the objective is to reveal the $\{\theta,t_x,t_y\}$ that satisfies (4) in the least mean squares sense. An initial value of $\{\theta,t_x,t_y\}$ can be estimated by solving the following linear equation:

$$\begin{bmatrix} \dots & \dots & \dots & \dots \\ x_{og(i)} & -y_{og(i)} & 1 & 0 \\ y_{og(i)} & x_{og(i)} & 0 & 1 \\ \dots & \dots & \dots & \dots \end{bmatrix} \begin{bmatrix} \cos\theta \\ \sin\theta \\ t_x \\ t_y \end{bmatrix} = \begin{bmatrix} \dots \\ x_{ov(i)} \\ y_{ov(i)} \\ \dots \end{bmatrix} \quad (5)$$

Afterward, an iterative refinement is carried out. At each iteration step, the non-linear function '$\cos\theta$' and '$\sin\theta$' are locally linearized with last estimate of θ; the increment of θ and new $\{t_x,t_y\}$ are computed by solving a linear equation:

$$\begin{bmatrix} \dots & \dots & \dots \\ -x_{og(i)}\sin\theta_{k-1} - y_{og(i)}\cos\theta_{k-1} & 1 & 0 \\ x_{og(i)}\cos\theta_{k-1} - y_{og(i)}\sin\theta_{k-1} & 0 & 1 \\ \dots & \dots & \dots \end{bmatrix} \begin{bmatrix} \Delta\theta_k \\ t_x \\ t_y \end{bmatrix} = \begin{bmatrix} \dots \\ x_{ov(i)} - x_{og(i)}\cos\theta_{k-1} + y_{og(i)}\sin\theta_{k-1} \\ y_{ov(i)} - x_{og(i)}\sin\theta_{k-1} - y_{og(i)}\cos\theta_{k-1} \\ \dots \end{bmatrix} \quad (6)$$

After the $\{\theta, t_x, t_y\}$ converge, the $\mathbf{R_{gv}}$ and $\mathbf{T_{gv}}$ are obtained. A piece of pseudo-code is given as follows:

Initialization: compute $\{\theta_{(init)}, t_{x(init)}, t_{y(init)}\}$ *using (5)*
Iteration: I. Linearize θ_{k-1}
II. Compute $\{\Delta\theta_k, t_x, t_y\}$ *using (6); let* $\theta_k = \theta_{k-1} + \Delta\theta_k$

By so far, all the spatial relationships among the CCS, the SCS, the GCS, and the VCS can be derived via (1).

4 The Improved Versions of the Comprehensive Extrinsic Calibration Method

The basic version of the comprehensive extrinsic calibration method is introduced in the previous section. Its performance depends on the accuracy of the camera intrinsic parameters which are not precisely known in practice. Concerning the calibration of the $\{\mathbf{R_{cs}}, \mathbf{T_{cs}}\}$, Zhang and Pless [12] propose a *global optimization* strategy which optimizes not only the $\{\mathbf{R_{cs}}, \mathbf{T_{cs}}\}$ but also the $\{\mathbf{A}, \mathbf{R_{p(i)c}}, \mathbf{T_{p(i)c}}\}$ ($\mathbf{A}$ is the camera intrinsic matrix) in a joint objective function:

$$\{\mathbf{R_{cs}}, \mathbf{T_{cs}}, \mathbf{A}, \mathbf{R_{p(i)c}}, \mathbf{T_{p(i)c}}\} = \arg\min_{\mathbf{R_{cs}}, \mathbf{T_{cs}}, \mathbf{A}, \mathbf{R_{p(i)c}}, \mathbf{T_{p(i)c}}} F_2 \quad (7)$$

$$F_2 = \sum_i \sum_j [\frac{\mathbf{N_{p(i)c}}}{\| \mathbf{N_{p(i)c}} \|} \cdot \mathbf{R_{cs}}^{-1}(\mathbf{M_{s(i,j)}} - \mathbf{T_{cs}}) - \| \mathbf{N_{p(i)c}} \|]^2 + \alpha \sum_i \sum_k \| \mathbf{m_{(i,k)}} - \mathbf{m}(\mathbf{A}, \mathbf{R_{p(i)c}}, \mathbf{T_{p(i)c}}, \mathbf{M_{p(i,k)}}) \|^2$$

where $\mathbf{m_{(i,k)}}$ and $\mathbf{m}(\mathbf{A}, \mathbf{R_{p(i)c}}, \mathbf{T_{p(i)c}}, \mathbf{M_{p(i,k)}})$ are respectively the extracted and projected image coordinates of the k-th control point for the $PCS_{(i)}$. This global optimization

strategy can be incorporated into the basic version of the calibration method to refine the calibration results. Therefore, an improved version of the comprehensive extrinsic calibration method is formed and is named the *improved version I* in this report.

The global optimization strategy in [12] over-adjusts the estimates of {$\mathbf{R_{cs}}$, $\mathbf{T_{cs}}$, $\mathbf{A}$, $\mathbf{R_{p(i)c}}$, $\mathbf{T_{p(i)c}}$} slightly to fit them to sensor data affected by noises; it results in a set of estimates that do not well satisfy the *ground plane constraint* introduced in Section III-B. To make the global optimization strategy more reasonable, the ground plane constraint is proposed to be taken into account as a term in the objective function, i.e. the third term of F_3 in (8) which stands for the summed square of distances of all the $\mathbf{O_{p(i)}}$ and $\mathbf{O_{p(i)}}+l\cdot\mathbf{X_{p(i)}}$ to the ground plane:

$$\{\mathbf{R_{cs}},\mathbf{T_{cs}},\mathbf{A},\mathbf{R_{p(i)c}},\mathbf{T_{p(i)c}},\mathbf{N_{Gc}}\} = \arg\min_{\mathbf{R_{cs}},\mathbf{T_{cs}},\mathbf{A},\mathbf{R_{p(i)c}},\mathbf{T_{p(i)c}}} F_3 \tag{8}$$

$$\begin{aligned} F_3 = & \sum_i \sum_j [\frac{\mathbf{N_{p(i)c}}}{\| \mathbf{N_{p(i)c}} \|} \cdot \mathbf{R_{cs}}^{-1}(\mathbf{M_{s(i,j)}} - \mathbf{T_{cs}}) - \| \mathbf{N_{p(i)c}} \|]^2 \\ & + \alpha \sum_i \sum_k \| \mathbf{m_{(i,k)}} - \mathbf{m}(\mathbf{A},\mathbf{R_{p(i)c}},\mathbf{T_{p(i)c}},\mathbf{M_{p(i,k)}}) \|^2 \\ & + \beta \sum_i \frac{\| [\mathbf{T_{p(i)c}}^{\mathrm{T}},1]\mathbf{N_{Gc}} \|^2 + \| [\mathbf{T_{p(i)c}}^{\mathrm{T}} + l\cdot\mathbf{e_1}^{\mathrm{T}}\mathbf{R_{p(i)c}}^{\mathrm{T}},1]\mathbf{N_{Gc}} \|^2}{\| \mathbf{N_{Gc}} \|^2} \end{aligned}$$

The Levenberg-Marquardt method [16] is used as the optimization technique. The α is a scalar weight which normalizes the relative contribution of the laser error term and the camera error term [12]. The scalar weight β is set to a comparatively large value and 100 in our implementation. The initial value of $\mathbf{N_{Gc}}$ is computed via (3), based on the initial estimates of {$\mathbf{A}$, $\mathbf{R_{p(i)c}}$, $\mathbf{T_{p(i)c}}$} The optimization strategy (8) is incorporated into the basic version of the calibration method, thus forming another improved version of the method which is referred to as the *improved version II* in this report.

5 Experimental Results

5.1 Synthetic Data Tests (Simulations)

The ground-truths of the CCS, the SCS, the GCS, and the VCS are set as follows in a global reference: the orientation and the position of the CCS are $[2.50, -2.50, 2.00]^{\mathrm{T}}$ rads and $[1.0, 0.0, 1.2]^{\mathrm{T}}$ meters; the orientation and the position of the SCS are $[-0.01, 0.03, 0.00]^{\mathrm{T}}$ rads and $[2.0, 0.0, 0.5]^{\mathrm{T}}$ meters; the orientation and the position of the VCS are $[0, 0, 0]^{\mathrm{T}}$ rads and $[0, 0, 0]^{\mathrm{T}}$ meters. With these ground-truths, the ground-truths of the GCS pose and the ground-truths of the spatial relationships among these coordinates systems can be derived.

The camera is configured according to an ideal pinhole model, with focal scaling factor 750 and principal point (384, 288). The chessboard pattern consists of 13×10 squares of 100mm×100mm size; the position of the squares is well registered in the PCS. The chessboard poses are generated randomly while satisfying two conditions: first, the chessboard bottom edge is on the ground plane; second, the chessboard can be perceived by both the camera and the 2D laser scanner. The chessboard orientation angle variation θ represents the angle between the chessboard plane and the image plane. Gaussian noise with mean 0 and standard deviation of 1.0 pixel is added to the projected image points. The laser points are computed based on the pose of the 2D laser scanner and the chessboard; they are contaminated by uniform noise within ±5cm, which fairly represents the error distribution of the real laser scanner in our tests.

In the experiments, the errors between the calibration results and the ground-truths are computed. First, the influence of the number of chessboard poses, of the chessboard orientation angle variation θ, and of the number of ground control points on the performance of the basic version of the calibration method will be examined. As the spatial relationships among the CCS, the SCS, and the GCS can be revealed based on the chessboard calibration practice only, the tests examine how the number of chessboard poses and the chessboard orientation angle variation θ influence the calibrated spatial relationships among the CCS, the SCS, and the GCS. As ground control points are necessary for revealing those spatial relationships associated with the VCS, the tests examine how the number of ground control points influences the calibrated spatial relationships associated with the VCS. Second, a performance comparison among the *basic version*, the *improved version I*, and the *improved version II* of the comprehensive extrinsic calibration method will be presented.

Performance w.r.t. the number of chessboard poses.

The influence of the number of chessboard poses on the calibrated $\mathbf{R}_{cg}$ and $\mathbf{T}_{cg}$ (CCS-GCS) and the calibrated $\mathbf{R}_{sg}$ and $\mathbf{T}_{sg}$ (SCS-GCS) is demonstrated. The poses number is varied from 5 to 16. For each poses number, 50 independent trials with θ=60^o are carried out; the RMS (root mean square) of the calibration errors of the 50 trials is computed and is shown in Fig.2. On the whole, the errors decrease as the number of chessboard poses increases.

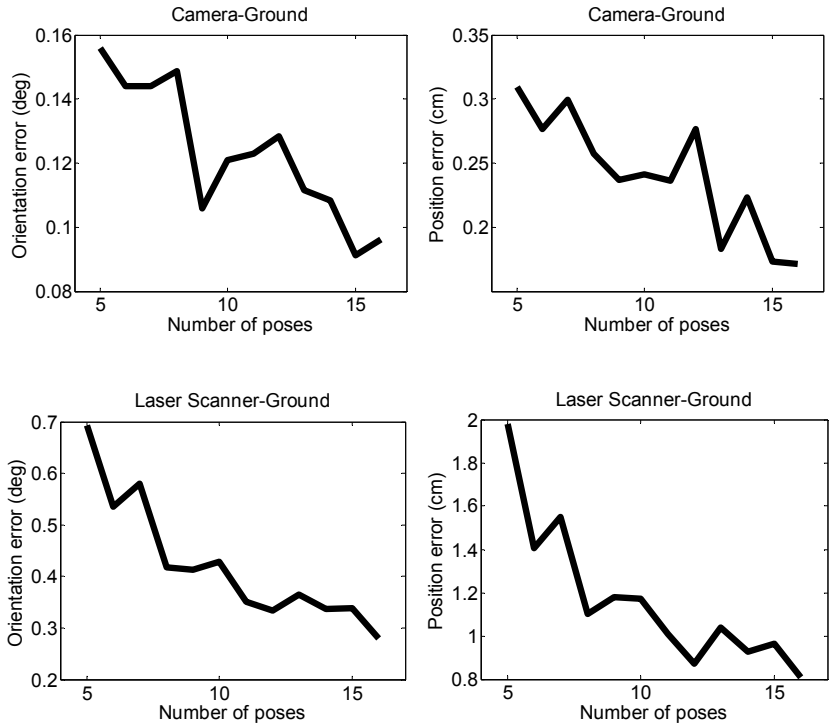

Fig.2. The influence of the number of chessboard poses

Performance w.r.t. the chessboard orientation angle variation

The influence of the chessboard orientation angle variation θ on the calibrated $\mathbf{R}_{cg}$ and $\mathbf{T}_{cg}$ (CCS-GCS) and the calibrated $\mathbf{R}_{sg}$ and $\mathbf{T}_{sg}$ (SCS-GCS) is demonstrated. The θ is varied from 20^o to 60^o every 2^o. For each θ, 50 independent trials are carried out. In each trial, 10 chessboard poses are randomly generated. The RMS of the calibration errors of the 50 trials is computed and is shown in Fig.3. On the whole, the calibration results improve as the θ increases until 50^o; afterward, the calibration results have no noticeable improvement.

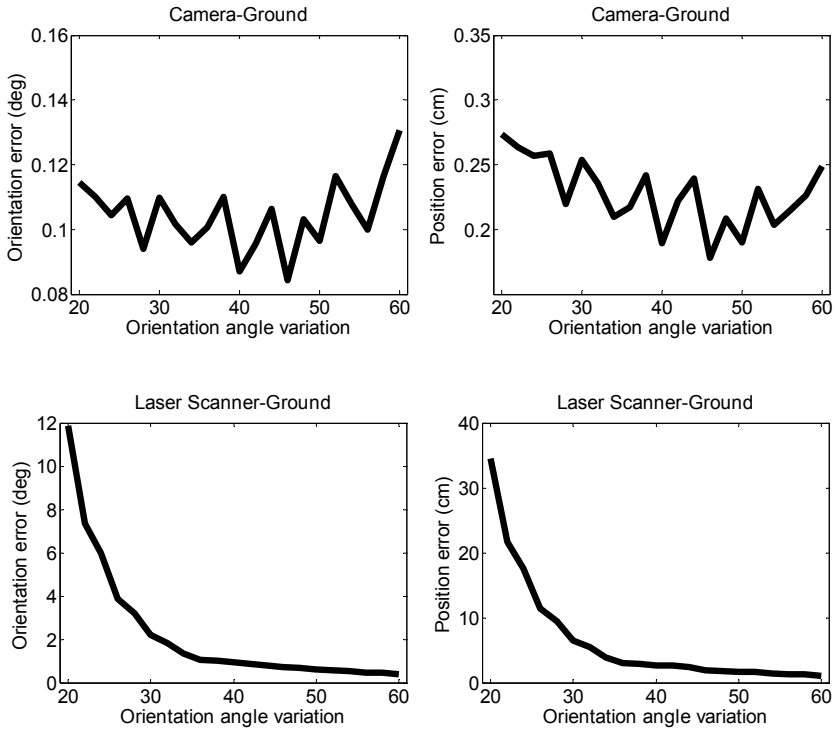

Fig.3. The influence of the chessboard orientation angle variation θ

Performance w.r.t. the number of ground control points

The influence of the number of ground control points on the calibrated $\mathbf{R}_{cv}$ and $\mathbf{T}_{cv}$ (CCS-VCS) and the calibrated $\mathbf{R}_{sv}$ and $\mathbf{T}_{sv}$ (SCS-VCS) is demonstrated. The number of ground control points is varied from 2 to 10. For each of these numbers, 50 independent trials with θ=60^o are carried out. In each trial, 10 independent and randomly generated chessboard poses are used. For each number, the RMS of the calibration errors of the 50 trials is computed and is shown in Fig.4; on the whole, the calibration errors decrease as the number of ground control points increases until 5; afterward, the calibration results have no noticeable improvement.

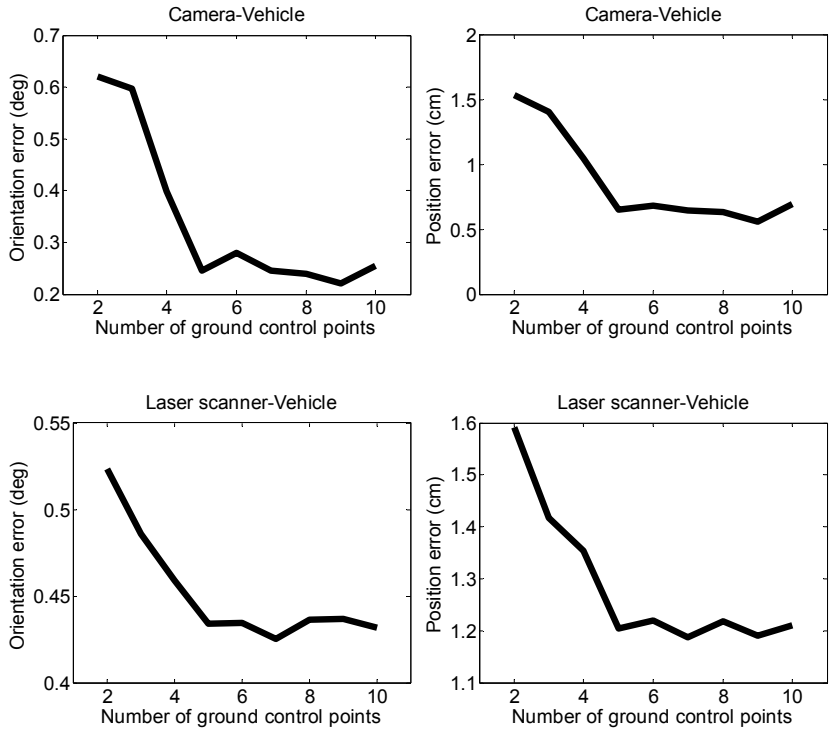

Fig.4. The influence of the number of ground control points

Performance comparison among the different method versions

This test demonstrates a performance comparison among the three versions of the comprehensive extrinsic calibration method (namely the *basic version*, the *improved version I*, and the *improved version II*).

During the test, 200 independent trials with θ ranging from 50^o to 60^o at random conditions are carried out. In each trial, 10 independent and randomly generated chessboard poses and 3 ground control points are used. The camera focal scaling factor is corrupted by Gaussian noise with mean 0 and standard deviation 10 pixels; the camera principal point is corrupted by Gaussian noise with mean 0 and standard deviation 5 pixels. In each trial, the three versions are applied to the same synthetic data (After some tuning according to the empirical rule that the α is a scalar weight which normalizes the relative contribution of the laser error term and the camera error term [12], the α is set to 0.013 for all the tests. The β is always set to 100); the calibration results are recorded respectively. After all the trials, the RMS of the calibration errors for each version is computed. The orientation (ori.) error is evaluated by the L2-norm error of the 3-vector associated with corresponding rotation matrix; the position (pos.) error is evaluated by the L2-norm error of corresponding translation vector. The improvement of the camera intrinsic matrix is evaluated by the ratio of the Frobenius

norm of the difference between the estimated **A** and the ground-truth to the Frobenius norm of the difference between the corrupted **A** and the ground-truth (This ratio is constantly 1 for the basic version). The results are listed in Table I.

Table I. The Performance Comparison Among the Three Versions

	Basic version	Improved version I	Improved version II
Ori. Error $\mathbf{R}_{cs}$ (deg)	1.158 [12]	0.964 [12]	0.894
Pos. Error $\mathbf{T}_{cs}$ (cm)	4.119 [12]	2.373 [12]	2.205
Ori. Error $\mathbf{R}_{cg}$ (deg)	0.534	0.226	0.193
Pos. Error $\mathbf{T}_{cg}$ (cm)	0.609	0.131	0.083
Ori. Error $\mathbf{R}_{sg}$ (deg)	0.556	0.479	0.457
Pos. Error $\mathbf{T}_{sg}$ (cm)	3.650	1.638	1.486
Ori. Error $\mathbf{R}_{cv}$ (deg)	1.092	0.474	0.428
Pos. Error $\mathbf{T}_{cv}$ (cm)	3.994	1.175	0.943
Ori. Error $\mathbf{R}_{sv}$ (deg)	0.704	0.519	0.491
Pos. Error $\mathbf{T}_{sv}$ (cm)	2.480	1.665	1.613
A Error ratio	1.000 [12]	0.158 [12]	0.120

Concerning all the error terms in Table I, the *improved version I* yields improvements over the *basic version* and the *improved version II* yields further improvements over the *improved version I*. The method in [12], which can only handle the calibration between the CCS and the SCS, forms the basis of this part of calibration for the *basic version* and the *improved version I*; its outputs are marked in Table I. As can be seen (error $\mathbf{R}_{cs}$, $\mathbf{T}_{cs}$, **A**), even only considering the calibration between the CCS and the SCS, the *improved version II* still outperforms the method in [12].

5.2 Real Data Tests

An IBEO laser scanner and a 1394 camera have been set up at fixed positions on a Citroen vehicle platform for tests. The angular resolution of the scan is 0.5 degree per measurement; the range measuring error varies within ±5cm. The camera image resolution is 768×576 pixels. The chessboard panel has a pattern consisting of 13×10 squares of 100mm×100mm size; the position of the squares is well registered on the chessboard. Since the squares are regularly arranged, this registration work can be easily performed. The calibration practice is carried out on our garage floor.

Since the ground-truth for real data is lacking, we can not directly evaluate the calibration errors of each trial. However, we follow a methodology of experimentation similar to those in [12] and [18]; the real-data tests are as follows:

24 images of the chessboard with different poses are taken, together with corresponding range readings, i.e. totally 24 calibration frames. In each trial, only 10 calibration frames are randomly selected and the three versions of the calibration method are applied to the same selected 10 calibration frames. We have carried out 200 independent trials. For each method version, we can not directly compute the RMS error as shown in Table I; instead, we compute the variance of the calibration results of the 200 trials—Despite that the trials variance is not strictly equivalent to their true RMS error; however, since the number of trials is large, the variance of such large amounts of trials can fairly reflect the error level of the calibration method and enables a reasonable comparison among the three method versions—The results are listed in Table II.

Table II. The variances of the Three Versions

	Basic version	Improved version I	Improved version II
Ori. Var $\mathbf{R}_{cs}$ (deg)	2.506 [12]	1.197 [12]	0.983
Pos. Var $\mathbf{T}_{cs}$ (cm)	8.439 [12]	4.522 [12]	3.846
Ori. Var $\mathbf{R}_{cg}$ (deg)	0.325	0.195	0.102
Pos. Var $\mathbf{T}_{cg}$ (cm)	1.345	0.187	0.143
Ori. Var $\mathbf{R}_{sg}$ (deg)	1.164	0.573	0.516
Pos. Var $\mathbf{T}_{sg}$ (cm)	5.583	3.332	2.97
Ori. Var $\mathbf{R}_{cv}$ (deg)	1.292	0.390	0.248
Pos. Var $\mathbf{T}_{cv}$ (cm)	5.328	1.803	1.533
Ori. Var $\mathbf{R}_{sv}$ (deg)	1.298	0.597	0.531
Pos. Var $\mathbf{T}_{sv}$ (cm)	6.414	3.282	2.919

As shown in the column of the *improved version II*, the calibration results of the 200 trials are rather consistent: the variances of the orientation terms are no more than one degree (most of them are around or less than half a degree); the variances of the position terms are no more than few centimeters. The calibration results of the *improved version I* are also rather consistent, only slightly outperformed by the *improved version II*. The consistency of the calibration results reflects the effectiveness of the proposed comprehensive extrinsic calibration method to reveal all the spatial relationships among the CCS, the SCS, the GCS, and the VCS.

Besides, even only considering the spatial relationships that the method in [12] can reveal (see variance $\mathbf{R}_{cs}$ and $\mathbf{T}_{cs}$), the *improved version II* still outperforms the method in [12].

Some intuitive results are also demonstrated to indirectly reflect the effectiveness of the proposed method (using the *improved version II*): First, the laser points and their ground projections are mapped onto the corresponding image, respectively marked by red points and blue points, as shown in Fig.5-Left. These mapped points are visually consistent with the environment shown in Fig.5-Left. Second, a bird-eye-view of the garage floor is generated based on the calibration results, as shown in Fig.5-Right. The squareness of the floor grids is well recovered.

The ground projections of the laser points can be positioned and the image of the garage floor can be inverse perspective mapped onto the ground, thanks to the calibrated spatial relationships among the CCS, the SCS, and the GCS, which are obtained by the proposed comprehensive extrinsic calibration method. It is worthy noting that these spatial relationships are revealed based on the common chessboard calibration practice without any extra calibration practice.

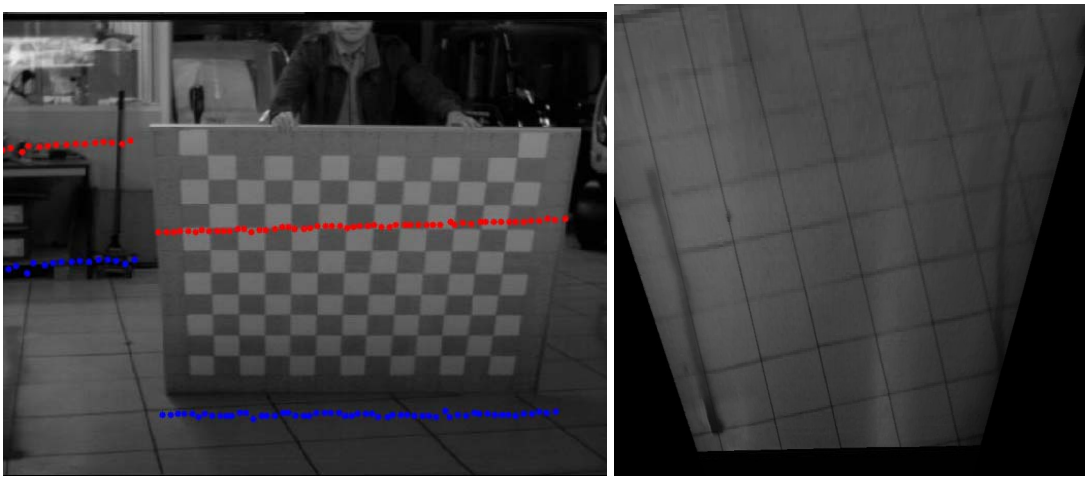

Fig.5. Intuitive effects: (Left) laser points and their ground projections; (Right) the bird-eye-view image of the garage floor

6 Conclusion

We propose a new method to perform comprehensive extrinsic calibration of a camera and a 2D laser scanner, i.e. the process of revealing all the spatial relationships among the CCS, the SCS, the GCS, and the VCS. As part of the method, the spatial relationships among the CCS, the SCS, and the GCS are calibrated based on the widely used chessboard calibration practice only. With few extra measurements, the spatial relationships associated with the VCS can be further revealed.

The proposed method has been tested on both synthetic data and real data: both quantitative evaluation and intuitive effects are given. Experiments have shown that the introduced comprehensive extrinsic calibration method can effectively reveal all the spatial relationships among the CCS, the SCS, the GCS, and the VCS. Besides, even only considering the spatial relationships that the method in [12] can reveal, the new method (the *improved version II*) still outperforms the method in [12]. The proposed method can serve as a desirable solution of camera and laser scanner calibration for mobile robotic applications; for example, the proposed method has been used for the calibration of the camera and the 2D laser scanner in the application presented in [17].
Recently, a new calibration method [18] has been proposed, which improves Zhang & Pless method [12] by reducing the number of poses needed to guarantee a desirable initial estimate. Our method improves Zhang & Pless method by extending its calibration capability (i.e. our method can reveal more spatial relationships than Zhang & Pless method does with the same calibration practice) and enhancing the calibration accuracy. This new method [18] and our method can complement each other and can be integrated, which would be a direction of further improvements.

Reference

[1] Gate G, Breheret A, Nashashibi F, "Centralized fusion for fast people detection in dense environment", *IEEE Int Conf on Robotics & Automation*, 2009, pp.76~81

[2] C. Premebida, O. Ludwig, U. Nunes, "LIDAR and vision-based pedestrian detection system", *Journal of Field Robotics*, vol.26, no.9, pp.696-711, 2009

[3] Y. Yemez, C.J. Wetherilt, "A volumetric fusion technique for surface reconstruction from silhouettes and range data", *Computer Vision & Image Understanding*, vol.105, no.1, pp.30-41, 2007

[4] Z. Kim, "Robust lane detection and tracking in challenging scenarios", *IEEE Trans on Intelligent Transportation Systems*, vol.9, no.1, pp.16-26, 2008

[5] M. Bertozzi, A. Broggi, "GOLD: A parallel real-time stereo vision system for generic obstacle and lane detection", *IEEE Trans on Image Processing*, vol.7, no.1, pp.62-81, 1998

[6] M. Bertozzi, A. Broggi, A. Fascioli, "Stereo inverse perspective mapping: theory and applications", *Image & Vision Computing Journal*, vol.16, no.8, pp.585-590, 1998

[7] P. Nunez, P. Drews Jr, R. Rocha, J. Dias, "Data fusion calibration for a 3d laser range finder and a camera using inertial data", *Proc. of 4th European Conf on Mobile Robots*, 2009, pp.31-36

[8] D. Scaramuzza, A. Harati, "Extrinsic self calibration of a camera and a 3d laser range finder from natural scenes", *IEEE Int Conf on Intelligent Robots & Systems*, 2007, pp.4164-4169

[9] C. Gao, J.R. Spletzer, "On-line calibration of multiple lidars on a mobile vehicle platform", *IEEE Int Conf on Robotics & Automation*, 2010, pp.279-284

[10] H. Aliakbarpour, P. Nuez, J. Prado, K. Khoshhal, J. Dias, "An efficient algorithm for extrinsic calibration between a 3d laser range finder and a stereo camera for surveillance", *Int Conf on Advanced Robotics*, 2009, pp.1-6

[11] H. Zhao, Y. Chen, R. Shibasaki, "An efficient extrinsic calibration of a multiple laser scanners and cameras sensor system on a mobile platform", *IEEE Intelligent Vehicles Symposium*, 2007, pp.422-427

[12] Q. Zhang, R. Pless, "Extrinsic calibration of a camera and laser range finder (improves camera calibration)", *IEEE/RSJ Int Conf on Intelligent Robots & Systems*, 2004, pp.2301-2306

[13] Z. Zhang, "A flexible new technique for camera calibration", *IEEE Trans on Pattern Analysis & Machine Intelligence*, vol.22, no.11, pp.1330-1334, 2000

[14] G. Li, Y. Liu, L. Dong, X. Cai, D. Zhou, "An algorithm for extrinsic parameters calibration of a camera and a laser range finder using line features", *IEEE Int Conf on Intelligent Robots & Systems*, 2007, pp.3854-3859

[15] O. Faugeras, "Three-dimensional computer vision: a geometric viewpoint", *MIT Press*, 1993

[16] J.J. More, "The Levenberg-Marquardt algorithm: implementation and theory", *G.A. Watson editor, Numerical Analysis, Lecture Notes in Mathematics*, 1977, Springer-Verlag, vol.630, pp.105-116

[17] H. Li, F. Nashashibi, "Multi-vehicle cooperative perception and augmented reality for driver assistance: a possibility to see through front vehicle", *IEEE ITSC*, 2011

[18] F. Vasconcelos, J.P. Barreto, U. Nunes, "A minimal solution for the extrinsic calibration of a camera and a laser-rangefinder", *IEEE Trans on Pattern Analysis & Machine Intelligence*, vol.34, no.11, pp.2097-2107, 2012

[19] V. Caglioti, A. Giusti, D. Migliore, "Mutual calibration of a camera and a laser rangefinder", *Int Conf on Computer Vision Theory & Applications*, 2008, pp.33-42

RESEARCH CENTRE
ROCQUENCOURT

Domaine de Voluceau
Rocquencourt BP 105
78153 Le Chesnay Cedex France

Publisher
Inria
Domaine de Voluceau - Rocquencourt
BP 105 - 78153 Le Chesnay Cedex
inria.fr